MIT Libraries | DSpace@MIT

MIT Open Access Articles

Entrance length effects on Graetz number scaling in laminar duct flows with periodic obstructions: Transport number correlations for spacer-filled membrane channel flows

Massachusetts Institute of Technology

Entrance length effects on Graetz number scaling in laminar duct flows with periodic obstructions: Transport number correlations for spacer-filled membrane channel flows

Wilko Rohlfs[a,b], John H. Lienhard V[a]

[a]*Department of Mechanical Engineering, Massachusetts Institute of Technology, Cambridge, MA 02139-4307, USA*
[b]*Institute of Heat and Mass Transfer, RWTH Aachen University, Augustinerbach 6, 52056 Aachen, Germany*

Abstract

Self-similarity and scaling laws are powerful tools in engineering and thus useful for the design of apparatus. This self-similarity is well understood for the heat and mass transfer in laminar empty channel flows, including the fully developed region as well as inlet length effects in the developing region (Graetz problem). In this study, we examine the validity of the scaling behavior arising from the Graetz solution for channel flows disturbed by periodic obstructions. Simulation results show that entrance length effects and scaling laws do not change due to the presence of obstructions if the flow field remains steady in time and the dimensionless inlet length is given by $X_\mathrm{T}/D_\mathrm{h} \approx C_\mathrm{inl.} \cdot \mathrm{Re} \cdot \mathrm{Pr}$, where $C_\mathrm{inl.} \approx 0.01$ for the local and $C_\mathrm{inl.} \approx 0.03$ for the average Nusselt number. The Nusselt number in the inlet region for an internal flow scales by $\mathrm{Nu} = (\mathrm{Re} \cdot \mathrm{Pr})^{1/3}$, similar to the empty channel flow (Shah and London, 1978). If the analogy between heat and mass transfer holds, same conclusions and relations are valid for the Sherwood number, $\mathrm{Sh} \propto (\mathrm{Re} \cdot \mathrm{Sc})^{1/3}$, where Sc denotes the Schmidt number. In the fully developed region, the Nusselt number depends slightly on the Reynolds and Prandtl numbers owing to the loss in self-similarity of the velocity field (contrary to the empty channel flow). The limit of the classical self-similarity is the onset of temporal oscillations (instability) in the flow field. Beyond this limit, the length of the thermal entrance region is strongly reduced. Furthermore, a strong dependency of the Nusselt number in the fully developed region on the Prandtl number is found.

Keywords: Laminar duct flow, Heat transfer coefficient, Mass transfer coefficient, Nusselt number correlation, Prandtl number, Numerical simulation, Sherwood number, Schmidt number

Nomenclature

c_p	specific heat capacity	[J/kgK]
D_h	hydraulic diameter	[m]
D_s	spacer diameter	[m]
$\mathcal{D}$	mass diffusivity	[m²/s]
h	heat transfer coefficient	[W/m²K]
H	channel height	[m]
k	thermal conductivity	[W/mK]
k_c	transfer coefficient	[m/s]
L_s	spacer separation distance	[m]
p	pressure	[kg/ms²]
q	specific heat flux	[W/m²]
t	time	[s]
T	temperature	[K]
u	velocity	[m/s]
x	streamwise coordinate	[m]
y	crosswise coordinate	[m]
α	thermal diffusivity	[m²/s]
δ	hydrodynamic b.l. thickness	[m]
δ_T	thermal b.l. thickness	[m]
ρ	density	[kg/m³]
ν	kinematic viscosity	[m²/s]

Dimensionless numbers

$\mathrm{Nu} = \frac{h D_h}{k}$	Nusselt number
$\mathrm{Pe} = \mathrm{Re} \cdot \mathrm{Pr}$	Peclet number
$\mathrm{Pr} = \frac{\nu}{\alpha}$	Prandtl number
$\mathrm{Re} = \frac{u_0 D_h}{\nu}$	Reynolds number
$\mathcal{R}e = \frac{u_0 D_s}{\nu}$	Reynolds number
$\mathrm{Sc} = \frac{\nu}{\mathcal{D}}$	Schmidt number
$\mathrm{Sh} = \frac{k_c D_h}{D}$	Sherwood number

Subscripts

0	reference value
q	constant heat flux b.c.
T	constant temperature b.c.
W	Wall
$\overline{}$	spatially averaged quantity

1. Introduction

Heat and mass transport in laminar forced convection channel flows occurs in many processes and thus has been widely investigated theoretically, experimentally, and numerically. Many literature reviews have been written (for instance the book by Shah and London reviewing analytical solutions for laminar channel flows [1]) and the fundamentals of laminar convective flows in circular ducts are addressed in standard heat transfer textbooks [2–4]. Thus, approximate solutions of the velocity and temperature profiles in the developing and fully developed regions are well known. The complexity of the problem increases for non-circular cross-sections [5] or flows inside concentric annuli [6, 7], non-Newtonian fluids or temperature dependent fluid properties [8], buoyancy forces (mixed convection), and more complex thermal boundary conditions (temporally or spatially varying) at the channel walls [9, 6, 7] or the channel inlet [10]. For many laminar flow configurations, analytical solutions of the Graetz problem are given in literature. Further, also for turbulent flow conditions analytical solutions are possible, assuming a turbulent velocity profile together with a distribution of the eddy diffusivity [11, 12]. An increasing interest in laminar flow regimes is also driven by the investigation of microchannels, such that Graetz number scaling behavior can be found in many correlations developed for heat and mass transfer in single phase microchannel flows [13]. Even the thermal development of forced convection flows through porous materials can be described by the Graetz number [14–16]. Thereby, Nield et al. [14] showed that the developing Nusselt number varies only slightly with the Darcy number but quiet drastically with the Peclet number, owing to the influence of axial conduction.

The motivation of this study is driven by the mass transfer in laminar forced convection channel flow that is typical for membrane technologies such as electrodialysis, reverse osmosis, ultrafiltration [17], and nano-filtration [18]. The channels of these modules are filled with mesh spacers, which separate the membrane walls of feed flow and permeate thus creating a flow passage. The spacers usually consist of crossed, almost cylindrical filaments which can be woven or non-woven. Besides their primary task of separating the membrane walls, they should also promote mass transfer, reduce fouling and reduce the phenomenon of concentration polarization near the membrane walls. The enhancement of transport (mass or heat) in internal flows is a general topic and not only addressed in membrane channel flows. Thus, various methods have been proposed in literature, ranging from twisted tapes [19], internal fins, wire coil, mesh or brush inserts, up to displaced mixing devices such as spaced disks, spaced streamline shapes, flow twisting device [20] or louvered stripes, for a review of heat transfer enhancing methods see [21–24]. A second characteristic of the mass transfer in membranes is the high Schmidt number, in the order of thousand for system feed waters [25]. Owing to the high Schmidt number, this transport is dominated by convection.

In recent years, many theoretical, experimental and numerical studies have been conducted with the aim of understanding the flow phenomena involved in laminar forced convection in spacer-filled ducts, as reviewed in Karabelas et al. [18]. Further, optimization of the spacer configuration has been addressed, whereby the desired enhancement in mass transfer is directly coupled to an undesired increase in pressure drop. Despite the large number of studies in this field, little attention is drawn to entrance length effects. It is commonly assumed that "the effect is less important when spacers are involved as they introduce a break-up of the boundary layer on the spacer dimension ..." [26].

However, it is well known from laminar plane channel flows that the dimensionless transport number (Nusselt or Sherwood number) approaches a constant value, after some entry length in which the boundary grows, that is independent of Reynolds and Prandtl numbers. Thus, the question arises: due to which mechanisms and at which critical obstacle or spacer dimensions (size and separation distance) does the scalar transport in a spacer-filled channel flow deviate from the scalar transport in a plane channel flow?

The remainder of this paper is structured as follows. Section 2 provides a general description of the hydrodynamic case studied, introducing the governing equations and relevant dimensionless numbers. Section 3 gives a short overview of the numerical methods used and presents a grid dependency analysis showing the robustness of the results obtained. Before discussing the results obtained for the spacer-filled channel, scaling laws in laminar developing plane channel flows are briefly recalled in section 4. Although this section presents well-known text book information, its content is essential for understanding more complex flow configurations. The main contribution of this paper is in section 5, which provides simulation results and a general understanding of the physical mechanisms involved in the developing channel flow with periodic obstacles. The results section is followed by a short discussion of the results with respect to membrane channel flows in section 6. Further, the new insights provided by this study are used to discuss the results obtained in earlier experimental and numerical studies and to provide guidelines for further investigations. Finally, section 7 summarizes the findings.
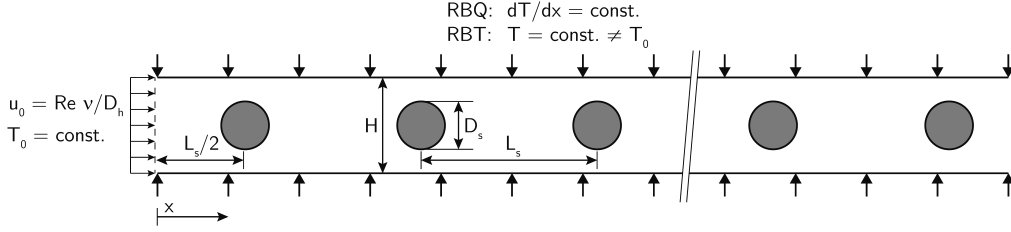
Figure 1: Schematic drawing of a heated duct flow interrupted by periodically spaced obstacles.

2. Problem statement, dimensionless parameters, and governing equations

The configuration of the channel flow investigated in this study is schematically shown in Fig. 1. An infinite width of the channel is assumed that allows for two-dimensional simulations. This assumption neglects crosswise and three-dimensional perturbations, limiting the validity of the simulation results to low Reynolds number cases. Note that a transition to three-dimensional wake regime is found to occur for the unconfined flow across a cylinder at $\mathcal{R}e = 180 - 194$ (defined later), depending on experimental conditions [27]. The length of the entire duct is chosen to be sufficiently long in order to investigate inlet length effects, but also to allow for fully resolved numerical simulations to be conducted in a reasonable time. In this study, most of the results for the inlet behavior are computed using a duct length of 200 successive spacers. The number of possible flow configurations is reduced by limiting the investigation to obstacles located in the center of the duct. However, many of the conclusions obtained for centered obstacles are also valid for off-center or wall-aligned obstacles.

Using the Einstein summation rule the governing equations for a time-dependent flow of an incompressible fluid with constant properties are

$$\frac{\partial u_i}{\partial t} + u_j \frac{\partial u_i}{\partial x_j} = -\frac{1}{\rho} \frac{\partial p}{\partial x_i} + \nu \frac{\partial^2 u_i}{\partial x_j \partial x_j} \tag{1}$$

and

$$\frac{\partial u_i}{\partial x_i} = 0, \tag{2}$$

where u denotes velocity, t time, x spatial coordinate, ρ density, p pressure, and ν the kinematic viscosity of the fluid. The energy equation reads

$$\frac{\partial T}{\partial t} + u_j \frac{\partial T}{\partial x_j} = \frac{k}{\rho c_{\mathrm{p}}} \frac{\partial^2 T}{\partial x_j \partial x_j}, \tag{3}$$

where k is the thermal conductivity, ρ is the density, and c_{p} is the specific heat capacity of the fluid.

In dimensionless form, the problem is described by a set of parameters involving fluid properties, geometric ratios and the characteristic velocity. The Reynolds number, describing the ratio between inertial and viscous forces is given by

$$\mathrm{Re} = \frac{u_0 D_{\mathrm{h}}}{\nu}, \tag{4}$$

where u_0 denotes the mass averaged velocity in the channel flow, and D_{h} the hydraulic diameter. Here, the hydraulic diameter is based on the channel height, i.e. $D_{\mathrm{h}} = 2H$, in agreement with the definition of the hydraulic diameter for infinite parallel plates without obstacles [2]. Note that various other definitions for the hydraulic diameter in channel flows with obstacles exist, e.g., based on the diameter of the obstacle [28] or based on the free passage (area or volume) [29, 30].

The Prandtl number describes the ratio between viscous diffusion and thermal diffusion

$$\mathrm{Pr} = \frac{\nu}{\alpha} = \frac{\nu \rho c_{\mathrm{p}}}{k}, \tag{5}$$

4

where $\alpha = k/(\rho c_\mathrm{p})$ is the thermal diffusivity. Similar to the Prandtl number in heat transfer, the Schmidt number describes the ratio between viscous diffusion and molecular diffusion (mass transfer)

$$\mathrm{Sc} = \frac{\nu}{\mathcal{D}}, \tag{6}$$

where $\mathcal{D}$ is the mass diffusivity of the species diffusing into the liquid.

Besides these property and flow-rate dependent dimensionless numbers, two dimensionless geometric ratios, the dimensionless channel height H/D_s and the dimensionless separation distance $L_\mathrm{s}/D_\mathrm{s}$, are used.

A result of the numerical simulations is the dimensionless heat or mass transfer coefficient, also known as the Nusselt or Sherwood number, respectively. In the remainder of this article, the analogy between heat and mass transfer is assumed to hold. This analogy is valid for low mass transfer rates and in the absence of buoyancy forces when the same type of boundary conditions are applied to either scenario. However, more studies and textbooks deal with heat transfer in developing channel flows, so all results are presented in terms of dimensionless temperature and heat transfer coefficient.

The local wall-side Nusselt number is defined by

$$\mathrm{Nu}_x = \frac{q_\mathrm{W}(x)D_\mathrm{h}}{k(T_\mathrm{W}(x) - \overline{T}(x))} = \frac{h(x)D_\mathrm{h}}{k}, \tag{7}$$

where $q_\mathrm{W}(x)$ is the wall-side heat flux (defined positive if the heat flux is from the wall to the fluid), T_W is the wall temperature, and h is the convective heat transfer coefficient. The latter is defined by

$$h(x) = -\frac{\left.\frac{\partial (T(x))}{\partial \vec{n}}\right|_\mathrm{W}}{(T_\mathrm{W}(x) - \overline{T}(x))} k. \tag{8}$$

Therein, $\vec{n}$ denotes the normal vector pointing from the wall towards the fluid and $\overline{T}(x)$ denotes the local caloric mean bulk temperature

$$\overline{T}(x) = \frac{\int_H u(x, y)T(x, y)dy}{\int_H u(x, y)dy}. \tag{9}$$

For constant heat flux boundary conditions, the overall Nusselt number for the entrance region from the beginning of the duct to the streamwise position x is defined by

$$\overline{\mathrm{Nu}}_{0 \to x, q} = \frac{q_{0 \to x}D_\mathrm{h}}{k\Delta T_\mathrm{avg}}, \tag{10}$$

with the average surface temperature

$$\Delta T_\mathrm{avg} = \left[\frac{1}{x}\int_0^x \frac{dx^*}{T_0(x) - \overline{T}(x)}\right]^{-1}. \tag{11}$$

For the constant temperature boundary condition, the overall Nusselt number for the entrance region from the beginning of the duct to streamwise position x is defined by

$$\overline{\mathrm{Nu}}_{0 \to x, T} = \frac{\overline{q}_{0 \to x}D_\mathrm{h}}{k\Delta T_\mathrm{lm}} = \frac{\overline{h}D_\mathrm{h}}{k}, \tag{12}$$

with $\overline{q}_{0 \to x}$ being the average heat flux and ΔT_lm being the logarithmic mean temperature

$$\Delta T_\mathrm{lm} = \frac{\left[T_\mathrm{W} - \overline{T}(0)\right] - \left[T_\mathrm{W} - \overline{T}(x)\right]}{\ln\left[\left(T_\mathrm{W} - \overline{T}(x)\right)/\left(T_\mathrm{W} - \overline{T}(0)\right)\right]}. \tag{13}$$

In a similar way, the dimensionless mass transfer coefficient (Sherwood number) is defined as $\mathrm{Sh} = k_c D_\mathrm{h}/\mathcal{D}$, where k_c in $\mathrm{m/s}$ is the local transfer coefficient and the driving potential for the diffusive transport is the gradient of the concentration.

3. Numerical approach

For the numerical investigation of a duct flow with periodically spaced obstacles the full incompressible Navier-Stokes equations are solved by the finite volume method employed in the open-source software package OpenFOAM[1] (version 2.3). For the steady-state cases, the SIMPLE algorithm (Semi-Implicit Method for Pressure Linked Equations) has been utilized while for the time-dependent cases the PIMPLE algorithm was used [31]. Results for the hydrodynamically and thermally fully developed region (see Fig. 7) are obtained using periodic boundary conditions and the method proposed by Patankar [32] for the constant heat flux boundary condition. In this method, the temperature is divided into a periodic and a non-periodic part. Therein, the non-periodic part of the temperature field accounts for the continuous raise in temperature, whereas the periodic part accounts for spatial variations.

$$T(x, y) = \gamma x + \hat{T}(x, y), \tag{14}$$

where γ is the change in temperature between entrance and exit of the periodic domain (here assumed to be in x-direction) and $\hat{T}$ denotes the periodic part of the temperature field. If a constant heat flux boundary is applied, γ is given by the ratio between the total heat flux (across both the upper and lower boundaries) and the heat capacity rate of the fluid

$$\gamma = \frac{T(x, y) - T(x + L, y)}{L} = \frac{q_{\mathrm{W}}}{\rho \bar{u} c_{\mathrm{p}} H}, \tag{15}$$

where $\bar{u}$ is the average velocity, H is the channel height, and L is the expansion of one periodic element. Replacing the temperature in the steady-state energy equation results in

$$u_j \frac{\partial \hat{T}}{\partial x_j} + u_x \gamma = \frac{k}{\rho c_{\mathrm{p}}} \frac{\partial^2 \hat{T}}{\partial x_j \partial x_j}. \tag{16}$$

Note that the boundary conditions also change if the surface normal is not perpendicular to the x-direction, e.g. on the surface of the obstacles (spacers).

A one-way coupled scalar transport equation is solved for the temperature. The central differences scheme is used for all spatial discretization, and a first order bounded implicit scheme is applied for temporal discretization. The final residual for all quantities (pressure, velocity and temperature) has been set to 10^{-5}. Note that significantly different results (also showing a strong dependency on Prandtl number) were obtained for higher values of the final residual, not allowing for an adequate convergence.

The numerical mesh for the spatial discretization is based on a hexagonal grid of square cells. Based on this hexagonal mesh, the cylinders are extruded from a triangulated surface geometry and a mesh containing hexahedra and split-hexahedra is automatically generated using the application *snappyHexMesh*. In a final step, the near wall cells are refined in order to resolve the thin thermal boundary layer.

A grid dependency analysis of the numerical simulation is presented in Fig. 2 for two different Prandtl number values and the case specified in the caption of the figure. Both the local and the overall Nusselt number are shown in a linear plot giving evidence of the accuracy of the results with respect to the applied spatial discretization. Only small differences in the high Prandtl number case exist between the 75 cell grid and the 100 cell grid. Note that the number of cells refers to the spatial discretization across the channel height. Simulations on a high resolution grid (150 cells) revealed very good agreement with the 100 cell grid (not shown).

4. Scaling laws in laminar developing plane channel flows

Transport processes in laminar channel flows with various cross-sectional geometries have been examined theoretically and analytically for many decades and is as such a classical problem in heat transfer books [2]. The problem is segregated into the fully developed and developing flow regions (hydrodynamically and/or thermally). In both cases, the mean temperature of the fluid in a plane channel flow increases in the flow direction according to

$$\frac{d\bar{T}}{dx} = \frac{q(x)}{\rho c_{\mathrm{p}} H u_0}, \tag{17}$$

---

[1]www.openfoam.org
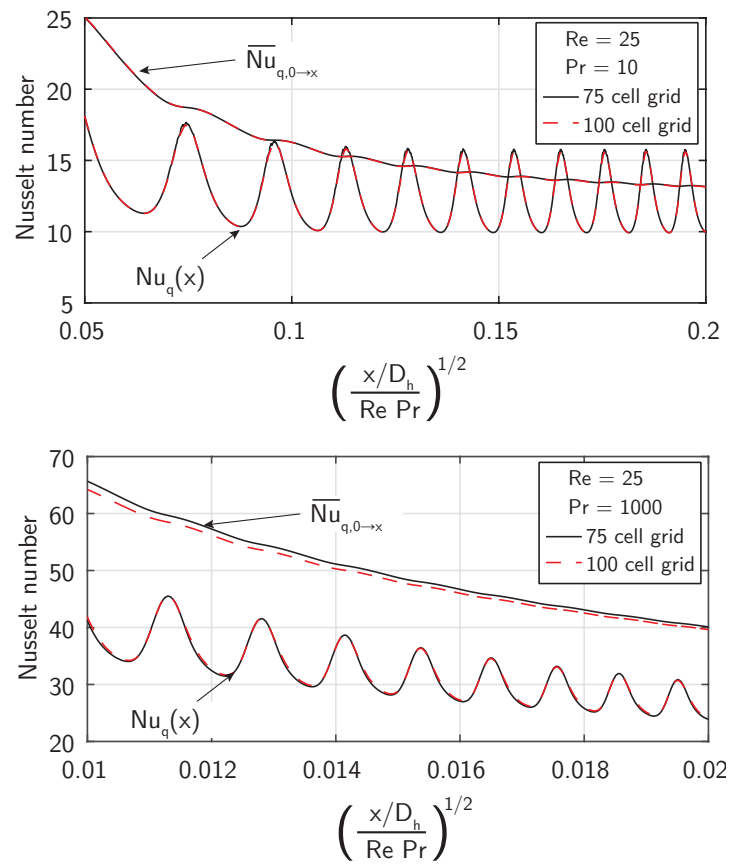
Figure 2: Grid dependency analysis for $Re = 25$, $H/D_s = 2$, and $L_s/D_s = 4$ and the constant heat flux boundary condition.
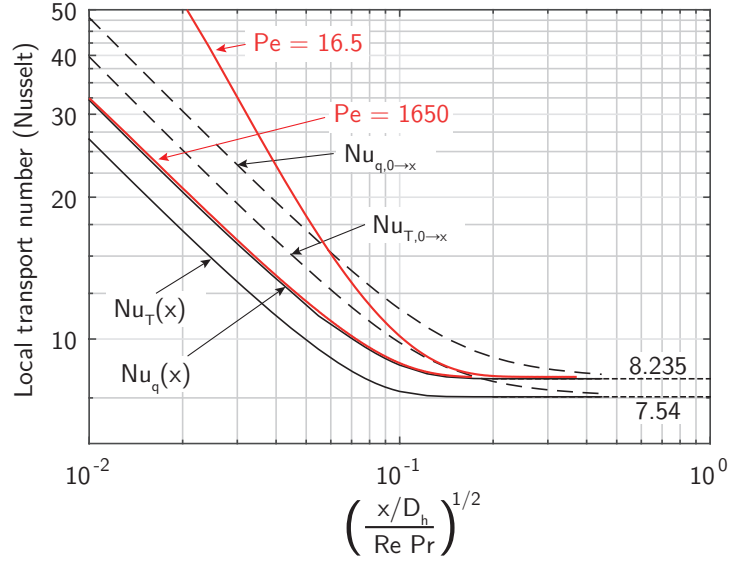
Figure 3: Heat transfer in the entrance region of a parallel-plate duct with constant heat flux: Black lines show results for an initially fully developed velocity profile and a large Peclet number (conduction in streamwise direction is negligible) based on data from Hwang and Fan [33] presented in the book of Shah and London [1]. Red lines show own results (DNS) for a Peclet number of Pe = 16.5 and Pe = 1650.

where $q(x)$ is the is the local heat flux per unit area.

A scaling analysis for the Nusselt number behavior on external and internal flows is provided in the textbook of Bejan [2]. Owing to a balance between streamwise convection and crosswise conduction, the two terms are required to be of the same order. From this and the inherent scale of the reference velocity U, a Prandtl dependency of the Nusselt number can be derived.

In case of laminar **internal flows** as considered in this study, the fully developed velocity profile spreads over the hydraulic length scale D_h. Thus, no free-stream velocity exist beyond the hydrodynamic inlet length and the velocity scale in the thermal boundary layer is the reference velocity itself. As a consequence, a Nusselt scaling of $Pr^{1/2}$ holds for both low and high Prandtl numbers [2] (contrary to the case of laminar external flows where the Prandtl number scaling changes from 1/3 for low Prandtl numbers to 1/2 for high Prandtl numbers), such that

$$\mathrm{Nu} \sim \left(\frac{x}{D_\mathrm{h}}\right)^{1/2} Pr^{1/2} \cdot Re^{1/2} \quad \text{(hydrodynamically fully developed internal flow).} \tag{18}$$

For further explanations the reader is referred to the aforementioned textbook [2]. Based on the above described behavior, a typical scaling for the streamwise direction of the thermally developing region is provided by

$$x^* = \frac{x}{D_\mathrm{h} \cdot \underbrace{Re \cdot Pr}_{Pe}}. \tag{19}$$

The black lines in Fig. 3 show the heat transfer in the thermal entrance region of a hydrodynamically fully developed duct flow in parallel plates without obstacles (Hagen-Poisseuille flow) for a large Peclet number (Pe = Re · Pr) at which conducion in streamwise direction is negligible. The plot is based on data from Hwang and Fan [33] presented in the book of Shah and London [1]. An alternative solution to the Greatz problem in the thermal inlet region is the asymptotic solution of Lévêque [34], showing that the velocity profile near the wall is very important for flows of large Prandtl number. The thermal entrance region in the dimensionless coordinate x^* is governed by a monotonically decreasing Nusselt number. The almost constant slope suggests the power law $\mathrm{Nu} \propto x^{*-1/3}$. The

transition from thermally developing to thermally fully developed flow occurs in the vicinity of $x^* \approx 0.01$. More precise values for the thermal entrance length can be given if somewhat arbitrary definitions like $\mathrm{Nu}^* = 1.05 \cdot \mathrm{Nu}_\infty$ are used[1]. However, a precise analysis of the entrance length is not in the scope of the present study, where attention is drawn to the physical effects and mechanisms. Owing to integration, the overall Nusselt number, $\overline{\mathrm{Nu}}_{0 \to x}$, approaches a constant value further downstream at $x^*_{0 \to x} \approx 0.03$. In the fully developed region, the Nusselt number is independent from Reynolds and Prandtl and takes a value of $\mathrm{Nu}_q = 8.235$ and $\mathrm{Nu}_T = 7.5407$ [12] for the constant heat flux and constant temperature boundary conditions, respectively.

In addition to the results from literature, our own simulation results for the empty channel and finite Prandtl numbers are shown by the red lines. Differences in the solution obtained from Hwang and Fan [33] are due to axial heat conduction, which is significant for low Peclet number cases, as shown in Haji-Sheikh et al. [35].

5. Scaling laws in laminar developing channel flows with periodic adiabatic obstacles

This section examines the entrance length behavior of a channel flow with periodic adiabatic obstacles using fully resolved numerical simulations. The first subsection investigates the regime of stationary flow conditions, occurring for low Reynolds number values only. For an increasing level of inertia (higher Reynolds number flows), the flow becomes unstable against infinitesimal disturbances leading – beyond a Hopf bifurcation [28] – to periodic two-dimensional oscillations. The heat transfer behavior in the entrance region for oscillating flow conditions is presented in subsection 5.2.

5.1. Influence on stationary flow conditions

The streamlines of the hydrodynamically fully developed flow are presented in Fig. 4 a) and b) for Re = 25 and Re = 100, respectively for constant heat flux conditions on the wall. The flow is two-dimensional, stationary, and non-mixing. For both flow conditions, streamlines are deformed by the cylinder and the fixed walls such that they approach each other, showing a local flow acceleration up to the position of maximal channel blockage ($x/D_h = 0$). For Re = 100, a stagnation point (illustrated by the black marker) is located on the centerline in the front part of the cylinder. Because of flow separation in the rear part of the cylinder, multiple stagnation points exist, located at the edges of the separation zone (black line) and again on the centerline of the cylinder. In contrast, there is no recirculation zone for Re = 25, whereas flow separation is known to occur already for a lower Reynolds number ($\mathcal{Re} = 6.25$) in case of an unbounded flow [36]. The delayed onset of flow separation can be attributed to the confinement of the flow, influencing the pressure field around the cylinder. Owing to the stationary characteristic of the flow, fluid in the recirculation zone behind the cylinder is endlessly trapped.

Figures 4 c) to f) illustrate the local temperature by isolines (top solid lines) and the heatlines (bottom dashed lines) according to their definition given in the textbook of Bejan [2]. Heatlines have the advantage of illustrating the actual direction of energy flow driven by convection and conduction, whereas isotherms are only appropriate to illustrate the driving potential for conduction.

For the case of high Peclet numbers, seen in Figs. d) to f), heatlines and streamlines are quasi-identical, meaning that convective transport in flow direction is orders of magnitude larger than diffusive transport normal to the stream-lines. Consequently, the temperature varies insignificantly in the streamwise direction, allowing for a separation of scales and a boundary layer-like approximation of the respective problem.

Furthermore, the temperature of the flow directed away from the wall is not significantly higher compared to the temperature of the flow directed towards the wall. Thus, convective transport from the wall to the center of the duct is of minor importance and the only mechanism allowing the mean channel temperature to increase is conduction in the normal direction to the streamlines, similar to the driving mechanism in the empty channel flow. Nevertheless, the Nusselt number in the channel flow with the obstacle is between 40% and 50% higher compared to the empty channel flow (Nu = 8.235), and depends on both the Reynolds and the Prandtl numbers. The main reason for this increase is found to be a redistribution of the velocity profile, leading on average to a higher near wall velocity. A further discussion on this effect is given in section 5.1.1.

Note that the above mentioned redistribution of the velocity profile is effectively a redistribution of the heat capacity, being convectively transported through the channel. In channel flows with nanoparticles, such a redistribution can also result from a non-homogenous distribution of particles as recently shown by Mahdavi et al. [37]. Additionally, a
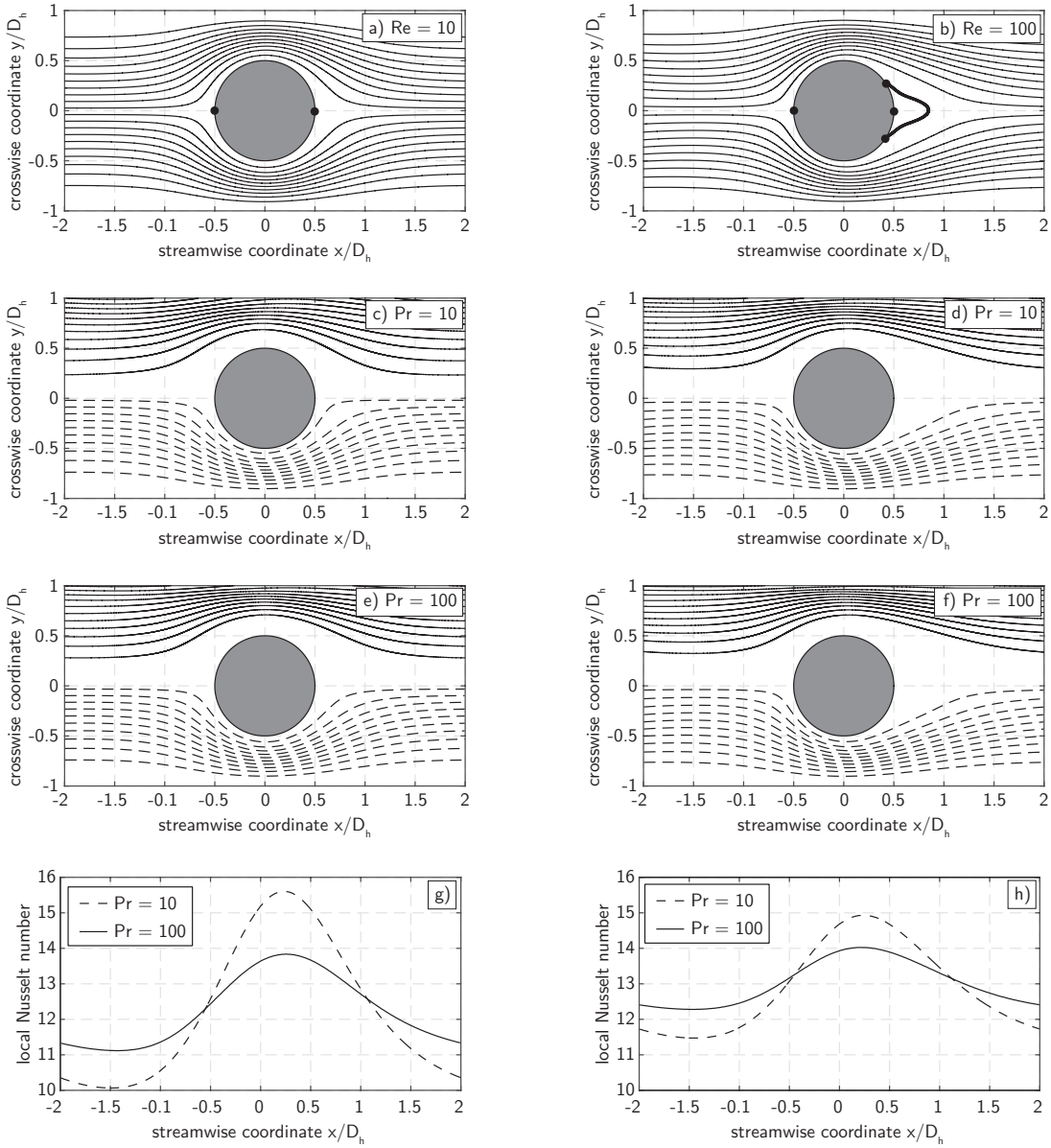
Figure 4: Illustration of the streamlines in the hydrodynamically and thermally fully developed region for Re = 25 (left) and Re = 100 (right). The thick black line corresponds to a stream function value of zero and encloses the separation zone while the black markers illustrate the stagnation points. Isolines and heatlines are shown for the constant heat flux boundary condition. The average Nusselt number of the four cases is $\overline{\mathrm{Nu}}(\mathrm{Re} = 25, \mathrm{Pr} = 10) = 11.81$, $\overline{\mathrm{Nu}}(\mathrm{Re} = 25, \mathrm{Pr} = 100) = 12.05$, $\overline{\mathrm{Nu}}(\mathrm{Re} = 100, \mathrm{Pr} = 10) = 12.56$, $\overline{\mathrm{Nu}}(\mathrm{Re} = 100, \mathrm{Pr} = 100) = 12.74$.

partial-slip boundary condition, caused by the addition of nano-particles, as discussed in Turkyilmazoglu [38] results in a redistributed velocity profile and thus contributes to an increase in Nusselt number.

The local Nusselt number distribution for the four different cases is presented in Figs. 4 g) and h). The amplitude of the local variation in the Nusselt number decreases with both Prandtl and Reynolds number. Consequently, the variations decrease with an increase in Peclet number. A first mechanism decreasing the amplitude is the reduction in thermal boundary layer thickness (which scales with Prandtl number) combined with the reduced deformation of

10

the streamlines and heatlines near the wall. Owing to this effect, the temperature variations are reduced and thus the amplitude of the Nusselt number. A second mechanism results from the increase in convective heat transfer with the Peclet number, reducing the streamwise temperature gradient. The decrease in amplitude with Prandtl number might suggests that local variations within the length-scale of the spacer separation distance do not play a significant role in membrane channel flows where the equivalent Schmidt number is of generally high magnitude. However, this statement is based on results for the constant flux boundary condition and an adverse effect will be shown in subsection 5.1.3.

Having examined the stationary flow conditions in the fully developed region, attention is now drawn on the development in the entrance region of the duct.
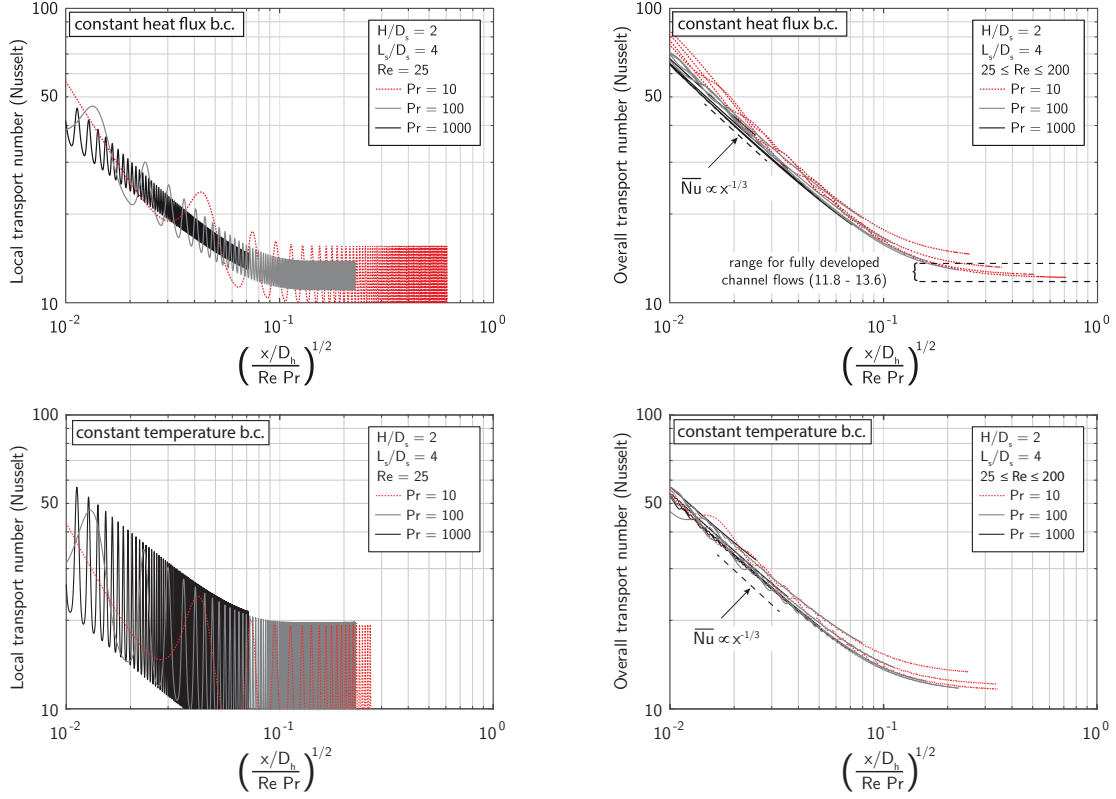
Figure 5: Local (left) and overall (right) dimensionless transport coefficient in the entrance region of a parallel-plate duct with periodic obstacles of geometric expansion $H/D_s = 2$ and $L_s/D_s = 4$. The range for fully developed channel flows (constant flux b.c.) is based on numerical simulations using periodic boundary conditions.

5.1.1. Effect of the Reynolds number

The Reynolds number affects the local and overall heat transfer coefficient in two different ways. First, the Reynolds number is a parameter scaling the hydrodynamic and thermal entrance length. Thus, the overall Nusselt number increases with an increase in Reynolds number for a constant physical channel length if the dimensionless length $x^* = x/(D_h \cdot Re \cdot Pr)$ is lower than 0.1 due to an extended entrance length. This effect is well known from the empty channel flow and results in a general scaling behavior of $Nu \propto Re^{1/3}$ because an in increase in Reynolds number decreases the dimensionless length x^*.

A secondary effect of the Reynolds number is caused by its influence on the flow field, as for instance seen by the extended length of the separation zone behind the cylinder (see Fig. 4b). This effect is not present in the empty channel, where the dimensionless velocity profile is self-similar and independent of the Reynolds number. As a consequence of the modified flow field, the distribution of the the velocity profile changes in such a way that the average velocity near the wall increases while the velocity in the center of the duct decreases. Owing to the redistribution of the velocity, the required diffusion length of heat decreases, thus increasing the Nusselt number. This effect is also present in the thermally fully developed channel flow such that deviations from the empty channel (Nu = 8.235) arise. Note that the redistribution of the velocity profile depends on the size, separation distance, and position of the obstacles. Thus, a redistribution in favor of a higher center velocity decreases the Nusselt number – as, for instance, seen in filaments adjacent to the wall in the study by Schwinge et al. [39].

5.1.2. Effect of the Prandtl number

The effect of the Prandtl number which – beside the Reynolds number – basically scales the diffusive to the convective transport is also twofold. First, the Prandtl number scales the hydrodynamic and thermal entrance length

12

in the same way as the Reynolds number such that Nu $\propto$ Pr$^{1/3}$. In an empty channel flow, the effect of the Nusselt and Prandtl numbers can be combined in the Peclet number as the flow field is self-similar with respect to variation in the Reynolds number. This is not possible for the case with periodic obstacle due to the missing self-similarity of the velocity profile with respect to the Reynolds number.

A secondary effect of the Prandtl number arises for low values of the Peclet number as shown by the red lines in Fig. 3 for the empty channel flow. For those cases, the influence of conduction in the streamwise direction becomes important, increasing the local Nusselt number in the entrance region due to backward diffusion (opposite to the flow direction). Contrary to this Nusselt number enhancement in the entrance region, forward diffusion decreases the average Nusselt number in the fully developed region as seen in Fig. 4 c). Here, heatlines and streamlines diverge in the wake of the cylinder, indicating an increased significance of the diffusive transport which reduces the gradient in the normal direction to the streamlines and thus the Nusselt number.

Further, the Prandtl number influences the periodic variations of the local transport number for the case of a constant heat flux as shown in the bottom right plot of Fig. 5. As expected, the periodic oscillations of the Nusselt number decrease with an increase in the Prandtl number for this boundary condition.

5.1.3. Effect of thermal boundary condition

For the empty channel flow, the type of boundary condition (constant heat flux or constant temperature) influences the local transport number. First, the boundary condition affects the steady state solution, such that the value for the constant heat flux (Nu = 8.235) is slightly higher than the value for the constant temperature (Nu = 7.5407). In a similar way, the transport number is influenced in the developing region. As a consequence, results in Fig. 3 appear to be almost parallel for the both boundary conditions. The same trend is evident in the right plots of Fig. 5 showing a similar difference in the overall Nusselt number for both types of boundary conditions.

A significant influence of the boundary condition exists in the local transport number (left plots). While the spatial variation in the Nusselt number decreases for higher Prandtl number for the constant heat flux boundary condition, this is not the case if a constant temperature is imposed. As a consequence, spatial variations with the length-scale of the spacer separation distance can play a significant role, depending on the kind of boundary condition. The type of boundary condition in membrane technologies is usually more complex and depends on the specific technology (membrane distillation, reverse osmosis, electrodialysis). In reverse osmosis for instance, water permeates through the membrane while the salt is rejected, causing an additional convective flux in normal direction and significant concentration polarization by the salt near the membrane wall. Thus, solutions for the mass transport in membranes are not necessarily bounded by the two boundary conditions. Owing to the complexity, the investigation of entrance length effects for specific membrane technologies exceeds the scope of this study.

5.1.4. Effect of geometric parameters

The geometric parameters varied in this study are the blockage ratio D_s/H and the separation distance between two spacers L_s/D_s. Because the Reynolds number has been studied before, this parameter has been fixed to a constant value of Re = 25. A low value for the Reynolds number has been chosen in order to reduce the effective length of the thermal entrance length. Two different Prandtl number values have been investigated. Figure 6 shows the overall transport number for Pr = 10 on the left side and for Pr = 1000 on the right side. Owing to the same physical length in both cases, results for Pr = 1000 are shown in the developing region ($x^* \ll 0.1$) only.

Simulation results reveal that the overall Nusselt number is significantly affected by the two geometric parameters. A general trend suggests that the overall Nusselt number increases with an increase in blockage ratio and a decrease in separation distance. This trend is expected and is caused by the redistribution of the velocity profile resulting in higher velocities in the near wall region. Nevertheless, the geometric parameter does not significantly influence the length of the entrance region or change the behavior of the developing thermal entrance region.

Simulation results for the fully developed region are presented in Fig. 7. Both plots show on the abscissa the ratio between the pressure difference of a channel with and without obstacles. On the ordinate, the Nusselt number ratio between the spacer-filled and empty channel is shown. Besides a variation of the two geometric parameters, the plots reveal results for a Reynolds number range from a value close to zero up to 200. The figures show that, unlike empty channel flows, the Nusselt number is dependent on the Reynolds number for fully developed channel flows with obstacles. In this case, the Nusselt number can vary by up to 50% in the range of the Reynolds numbers investigated.

Obviously, the influence of the Reynolds number as well as the deviations of the flow field from the empty channel flow increase with blockage ratio and are inversely proportional to the separation distance.

In contrast to the mild increase in the Nusselt number, the pressure drop rises significantly for the spacer-filled channel. For a blockage ratio of $D_s/H = 0.25$, the pressure drop increases by a factor between four and seven (Reynolds number and separation distance dependent). This high pressure drop can be compared to the artificial pressure drop that arises if the same flow rate would pass two channels which have together the height of the remaining cross sectional area of the spacer filled channel. For $D_s/H = 0.25$, this channel height is $D_{artificial}/H = 0.75/2$ while the average velocity in the duct is $U_{artificial} = 1.33 \cdot U$, revealing a pressure drop of $\Delta P_{artifical}/\Delta P_{empty} = 9.4$. Consequently, the periodic obstacles cause a pressure drop that is on the order of a channel flow with two no-slip boundary conditions and a height of the remaining cross-sectional area. In case of the high blockage ratio ($D_s/H = 0.75$), the pressure drop increases by 30 to 50 times compared to the empty channel, while the heat transfer coefficient increases only by a maximum of three. The graphs also reveal that the blockage ratio is the most significant parameter influencing the increase in pressure drop and that the influence of the Reynolds number is weak. However, the real pressure drop scales by the square of the velocity and is thus strongly dependent on the actual flow rate.

Owing to the logarithmic scale of the pressure drop and the linear scale of the Nusselt number, the plot reveals the high cost in terms of pumping power associated with the immersed obstacles without a significant change in the Nusselt number. Note that a comparison between different cross-sectional channel shapes is usually known to give a linear relation between transport coefficient and friction factor [2].

The sensitivity of the simulation results with respect to spacer positions is conducted by introducing a random deviation of the precise central spacer position. A relative bandwidth for the perturbation of 5 percent with respect to the channel height and the separation distance has been chosen for these tests. Simulation results indicate no significant deviations from the perfectly centered and separated spacers (not shown).

5.2. Influence of temporally oscillating flow conditions

The flow past a cylinder in unconfined and confined configurations is characterized by a cascade of transition as outlined in the review by Williamson [27]. For the unconfined case and very low Reynolds numbers ($Re = UD/\nu \ll 1$), the streamlines of the flow are aligned to the cylinder and symmetric to the center-axis. For higher but still low Reynolds numbers, flow separation in the rear part of the cylinder occurs and a separation bubble is formed which increases in size as the Reynolds number is increased. At a critical Reynolds number of $\mathcal{R}e_{crit.} \approx 46$ [27, 28], the flow becomes unstable forming the characteristic periodic and regular pairs of vortices in the wake of the cylinder, is the von Kármán vortex street. A further increase in the Reynolds number results in series of instabilities (bifurcations) leading to the formation of non-periodic, three-dimensional, and finally chaotic vortex motion in the wake of the cylinder.

A similar transition between the different flow regimes occurs for the confined case, where the cylinder blocks the flow passage. Two detailed numerical studies dealing with the flow past a single cylinder in a confined duct [40, 28] give interesting insights into the transitional behavior. First, it is found that the critical Reynolds number for the transition between the laminar steady regime and the regime of periodic laminar vortex shedding is shifted towards higher Reynolds numbers as the blockage ratio (D_s/H) increases. Thus, the flow becomes more stable against infinitesimal disturbances. A maximum value of the critical Reynolds number is found for $D/H \approx 0.5$ where $Re_{crit} \approx 110$ [28]. For higher blockage ratios, the value of the critical Reynolds number decreases slightly.

The critical values for the onset of unsteady periodic motions of a flow past a single cylinder in the center of a confined geometry can be used as a first approximation when an infinite number of cylindrical obstacles is considered. Koutsou et al. [41] for instance identified a critical Reynolds number of $Re_{crit} \approx 60$ in case of an blockage ratio of $D_s/H = 2$ and a separation distance of $L_s/D_s = 6$. This value is slightly lower compared to the single cylinder where $Re_{crit} \approx 83$. Although the critical Reynolds number is reduced for this specific case, a stabilizing mechanism can also be expected for other parameters (blockage ratio and separation distance) owing to the increase in flow confinement and thus viscous dissipation and perturbation dampening.

Note that the values of the critical Reynolds number given above increase by a factor of $2H/D$ if the definition of the Reynolds number given in eq. (4) is used. For the present case of $H/D_s = 2$ and $L_s/D_s = 4$, the onset of oscillatory flow conditions is expected to be above $Re = 200$. Thus, numerical simulations of a higher Reynolds number ($Re = 400$) have been conducted in order to investigate entrance length effect under oscillatory flow conditions.
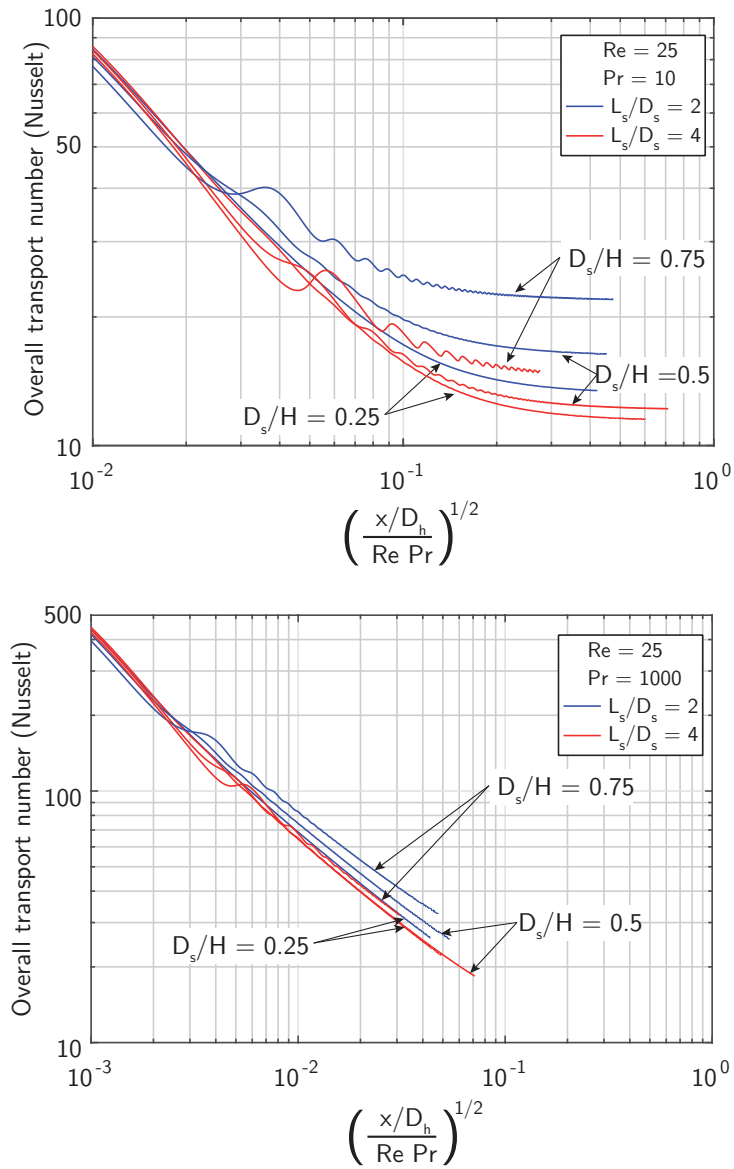
Figure 6: Overall dimensionless transport coefficient in the entrance region of a parallel-plate duct with periodic obstacles for Re = 25 and a variation of the geometric expansion $D_s/H = [0.25; 0.5; 0.75]$ and $L_s/D_s = [2; 4]$. The constant heat flux boundary condition is applied.
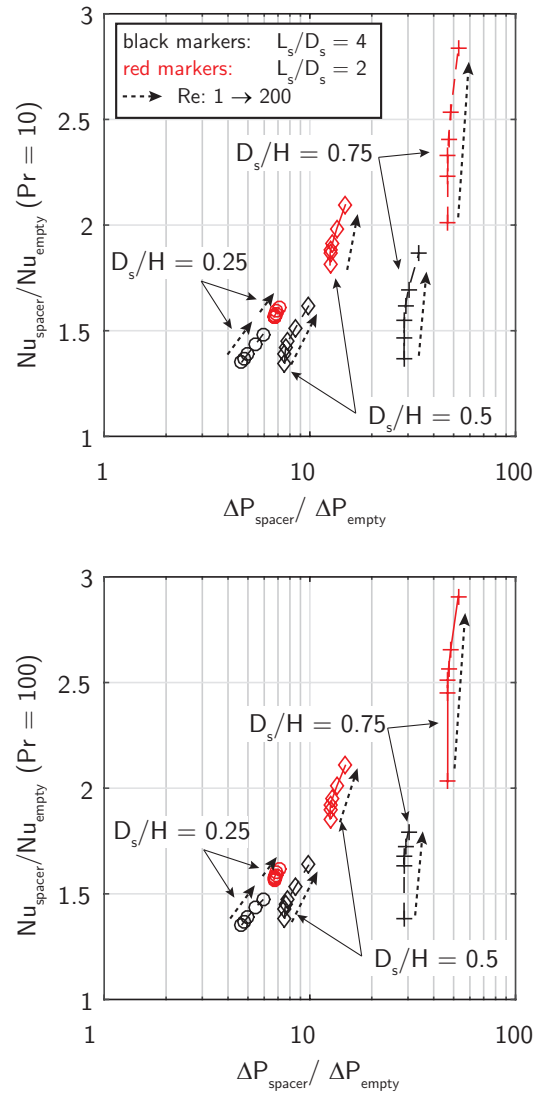
15

Figure 7: Comparison of pressure loss and overall dimensionless transport coefficient in the thermally and hydrodynamically fully developed region of a parallel-plate duct with periodic obstacles. The constant heat flux boundary condition is applied.
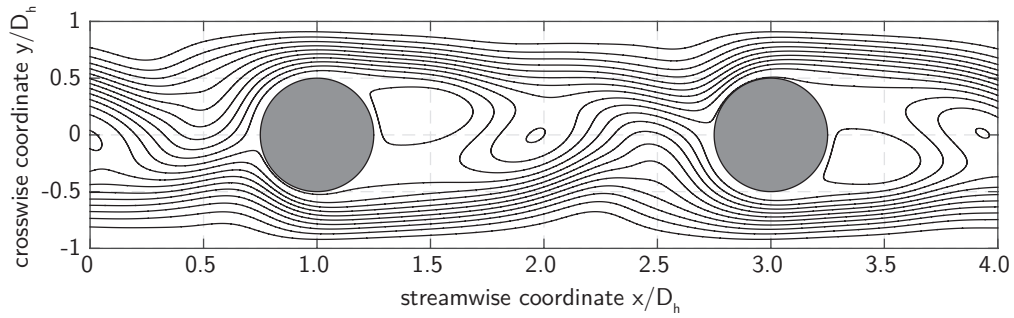
16

Figure 8: Plot of the instantaneous flow field by streamlines illustrating the oscillatory flow condition obtained for Re = 400 with periodic obstacles of geometric expansion $D_s/H = 0.5$ and $L_s/D_s = 4$.
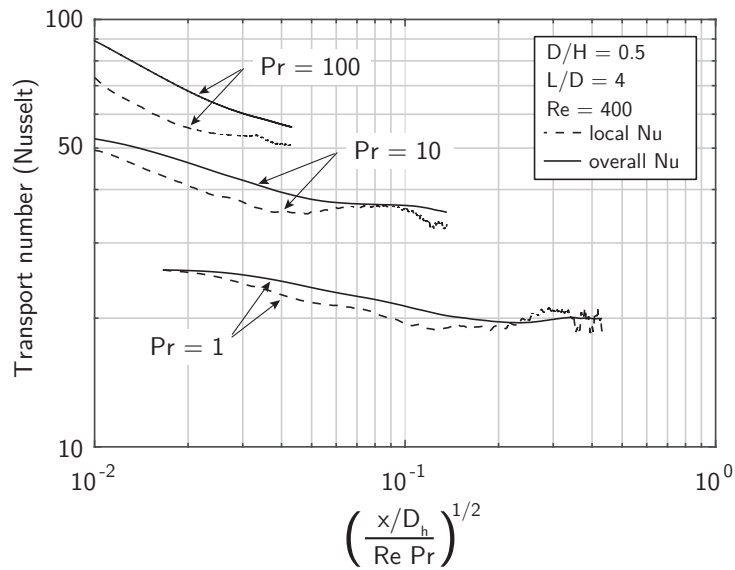

Figure 9: Local and overall dimensionless transport coefficient in the entrance region of a parallel-plate duct with periodic obstacles in the oscillating regime with Re = 400. Results are shown for the constant heat flux boundary condition and obtained from an instantaneous temperature field.

Figure 8 illustrates the instantaneous velocity profile for this flow configuration. The flow is characterized by periodic, alternating vortex shedding behind consecutive cylinders. In addition, wall attached vortices arise. These vortices are also found to periodically shed from the wall, thereby transporting warm liquid convectively to the center of the duct. In the dimensionless transport number plot presented in Fig. 9, a significantly different behavior is found for this flow condition. Self-similarity of the local and overall transport number with respect to the Prandtl number is lost and the transport number in the fully developed region converges to significantly different values depending on Prandtl number. As a consequence, the entrance length behavior is found to change between the steady and unsteady regime.

6. Guidelines for experimentalists and engineers designing apparatuses involving high Prandtl/Schmidt number channel flows

The long entrance length required in the stationary regime has some implications on experimental and numerical results presented in literature. The numerical results presented in Schwinge et al. [39] are based on a short channel with a maximum length of $L_s/H = 8$, high Schmidt numbers $100 < Sc < 50,000$ and a Reynolds number of 200. For the lowest Schmidt number examined, the thermal entrance length is $L_s/H = 200$, for which all the results fall in the range of the entrance length. His findings, that the mass transfer rate scales with Schmidt number in a spacer filled channel flow similar to empty channel flows are thus a result from the developing character of the boundary layer. Similar results have been obtained in the experimental study by Koutsou [25] for three-dimensional filaments. Owing to their ratio between channel length and height of $L/H = 20$, their high Schmidt numbers $Sc > 1450$, and the Reynolds number range from 25 to 180, all results are affected by the entrance length behavior. As a consequence the authors have identified an exponent for the Schmidt number between 0.38 and 0.48 (depending on the geometry of the spacer mesh) as well as a significant Reynolds number dependency ($0.56 < a < 0.87$). However, the information provided in the previously mentioned articles cannot be used for long channel flows, where the boundary layer exceeds the entrance length.

The physical insights gained in this study reveal that the break-down of the classical entrance length behavior is associated with a transition from a stationary to a time-dependent flow field. As a consequence, experimental and numerical studies on the effect of spacers should take into account this transition by characterizing the flow regime.

Finally, the transition between the stationary and time-dependent flow regime should be taken into account when optimizing the geometry of obstacles or spacers. A good performance in heat and mass transfer at a low pressure drop is thus expected for obstacle geometries which cause a transition to the time-dependent flow regime at the lowest Reynolds number. However, more detailed investigations are required in this context.

7. Summary and conclusions

This study investigated the entrance length effect in laminar channel flows with periodically spaced obstacles in dependence of the Reynolds number, Prandtl number, wall thermal boundary condition and obstacle geometry using numerical simulations. It was shown that the "classical" entrance length effect known from laminar flows in empty channels is also valid for flows influenced by the presence of obstacles if the flow field is of stationary (non-mixing) type. Thus, the entrance length effects have to be accounted for if the Greatz number $x/(D_h \cdot Re \cdot Pr)$ is smaller than 0.1. Although streamlines and heatlines are almost overlapping for high Peclet numbers, diffusion in the normal direction to the streamlines is the only mechanism contributing to an increase of the inner-channel temperature, similar to the transport in empty channel flows. This explains the validity of the classical entrance length scaling. The increase in the Nusselt number compared to the empty channel flow is caused by a redistribution of the flow field which itself is Reynolds-dependent. Although periodic spacers with a blockage ratio of $D_s/H = 0.5$ are found to increase the Nusselt number in the fully developed region by 50-100%, the influence of the Prandtl number is found to be weak $< 5\%$. The Reynolds number, which influences the shape of the flow field past the cylindrical obstacle varies the Nusselt number by $\pm 20\%$. This effect generally increases with the blockage ratio but shows adverse effects with respect to the separation distance.

A limit of the entrance length scaling is identified and coincides with the transition from a stationary to a transient flow regime. This transition to periodic vortex shedding arises in a channel flow configuration, however at a different

value of the critical Reynolds number. Beyond this transition, the self-similarity of the entrance length behavior is lost, causing an earlier transition to a thermally developed flow. Furthermore, the Prandtl number influence becomes significant in the fully developed region.

In terms of mass transfer in membrane channel flows where high Schmidt numbers are involved, the developing region of the concentration boundary can be of significant length, even exceeding the size of the membrane module. Thus, more emphasis should be drawn to identify the flow regime (stationary or transient) in experimental and numerical investigations and in the optimization of spacer geometries.

Spatial variations of the transport number caused by the periodically spaced obstacles are found to be significant if a Dirichlet boundary condition (constant value) is applied. For the case of a Neumann boundary condition (constant flux), spatial variations decrease with Prandtl/Schmidt number and are thus of minor importance. For the effect of concentration polarization in membrane processes, this adverse effect requires a closer examination of the exact boundary condition involved. This boundary condition is usually of Robin-type (third kind) and depends on the specific technology (membrane distillation, reverse osmosis, or electrodialysis).

Acknowledgements

References

[1] R. K. Shah, A. L. London, Laminar flow forced convection in ducts: A source book for compact heat exchanger analytical data, Academic Press, New York, 1978.

[2] A. Bejan, Convective Heat Transfer, John Wiley & Sons, Inc., 2013.

[3] R. B. Bird, W. E. Stewart, E. N. Lightfoot, Transport Phenomena, John Wiley & Sons, Inc., 2007.

[4] J. H. Lienhard IV, J. H. Lienhard V, A Heat Transfer Textbook, 4th Edition, Dover Publications, 2011.

[5] R. Shah, Laminar flow friction and forced convection heat transfer in ducts of arbitrary geometry, International Journal of Heat and Mass Transfer 18 (7) (1975) 849 – 862. doi:http://dx.doi.org/10.1016/0017-9310(75)90176-3.

[6] B. Weigand, F. Wrona, The extended graetz problem with piecewise constant wall heat flux for laminar and turbulent flows inside concentric annuli, Heat and Mass Transfer 39 (4) 313–320. doi:10.1007/s00231-002-0303-1.

[7] B. Weigand, K. Eisenschmidt, The extended graetz problem with piecewise constant wall temperature for laminar and turbulent flows through a concentric annulus, International Journal of Thermal Sciences 54 (2012) 89 – 97. doi:http://dx.doi.org/10.1016/j.ijthermalsci.2011.12.006.

[8] M. Shojaeian, A. Kosar, Convective heat transfer of non-newtonian power-law slip flows and plug flows with variable thermo-physical properties in parallel-plate and circular microchannels, International Journal of Thermal Sciences 100 (2016) 155 – 168. doi:http://dx.doi.org/10.1016/j.ijthermalsci.2015.09.024.

[9] W. Aung, Fully developed laminar free convection between vertical plates heated asymmetrically, International Journal of Heat and Mass Transfer 15 (8) (1972) 1577 – 1580. doi:http://dx.doi.org/10.1016/0017-9310(72)90012-9.

[10] G. Cossali, Analytical solution of graetz problem in pipe flow with periodic inlet temperature variation, International Journal of Heat and Mass Transfer 52 (1314) (2009) 3396 – 3401. doi:http://dx.doi.org/10.1016/j.ijheatmasstransfer.2009.02.028.

[11] B. Weigand, R. Bogenfeld, A solution to the turbulent graetz problem by matched asymptotic expansions for an axially rotating pipe subjected to external convection, International Journal of Heat and Mass Transfer 78 (2014) 901 – 907. doi:http://dx.doi.org/10.1016/j.ijheatmasstransfer.2014.07.057.

[12] B. Weigand, Analytical Methods for Heat Transfer and Fluid Flow Problems, Springer-Verlag Berlin Heidelberg, 2015. doi:10.1007/978-3-662-46593-6.

[13] M. Asadi, G. Xie, B. Sunden, A review of heat transfer and pressure drop characteristics of single and two-phase microchannels, International Journal of Heat and Mass Transfer 79 (2014) 34 – 53. doi:http://dx.doi.org/10.1016/j.ijheatmasstransfer.2014.07.090.
URL http://www.sciencedirect.com/science/article/pii/S0017931014006796

[14] D. Nield, A. Kuznetsov, M. Xiong, Thermally developing forced convection in a porous medium: parallel plate channel with walls at uniform temperature, with axial conduction and viscous dissipation effects, International Journal of Heat and Mass Transfer 46 (4) (2003) 643 – 651. doi:http://dx.doi.org/10.1016/S0017-9310(02)00327-7.

[15] M. Dehghan, M. Valipour, A. Keshmiri, S. Saedodin, N. Shokri, On the thermally developing forced convection through a porous material under the local thermal non-equilibrium condition: An analytical study, International Journal of Heat and Mass Transfer 92 (2016) 815 – 823. doi:http://dx.doi.org/10.1016/j.ijheatmasstransfer.2015.08.091.

[16] M. Dehghan, M. Valipour, S. Saedodin, Y. Mahmoudi, Investigation of forced convection through entrance region of a porous-filled microchannel: an analytical study based on the scale analysis, Applied Thermal Engineering (2016) – doi:http://dx.doi.org/10.1016/j.applthermaleng.2015.12.086.

[17] A. D. Costa, A. Fane, C. Fell, A. Franken, Optimal channel spacer design for ultrafiltration, Journal of Membrane Science 62 (3) (1991) 275 – 291. doi:http://dx.doi.org/10.1016/0376-7388(91)80043-6.

[18] A. Karabelas, M. Kostoglou, C. Koutsou, Modeling of spiral wound membrane desalination modules and plants review and research priorities, Desalination 356 (2015) 165 – 186, state-of-the-Art Reviews in Desalination. doi:http://dx.doi.org/10.1016/j.desal.2014.10.002.

[19] H. Bas, V. Ozceyhan, Heat transfer enhancement in a tube with twisted tape inserts placed separately from the tube wall, Experimental Thermal and Fluid Science 41 (2012) 51 – 58. doi:http://dx.doi.org/10.1016/j.expthermflusci.2012.03.008.

[20] J. Liu, A. Iranshahi, Y. Lou, G. Lipscomb, Static mixing spacers for spiral wound modules, Journal of Membrane Science 442 (2013) 140 – 148. doi:http://dx.doi.org/10.1016/j.memsci.2013.03.063.

[21] A. Jacobi, R. Shah, Heat transfer surface enhancement through the use of longitudinal vortices: A review of recent progress, Experimental Thermal and Fluid Science 11 (3) (1995) 295 – 309, generation and Structure of Vortical Flows for Heat Transfer Enhancement. doi:http://dx.doi.org/10.1016/0894-1777(95)00066-U.

[22] R. L. Webb, N.-H. Kim, Principles of Enhanced Heat Transfer, Taylor & Francis, 2005.

[23] A. Dewan, P. Mahanta, K. S. Raju, P. S. Kumar, Review of passive heat transfer augmentation techniques, Proc. Instn. Mech. Engrs. 218 (2004) 509–527.

[24] W.-T. Ji, A. M. Jacobi, Y.-L. He, W.-Q. Tao, Summary and evaluation on single-phase heat transfer enhancement techniques of liquid laminar and turbulent pipe flow, International Journal of Heat and Mass Transfer 88 (2015) 735 – 754. doi:http://dx.doi.org/10.1016/j.ijheatmasstransfer.2015.04.008.

[25] C. Koutsou, S. Yiantsios, A. Karabelas, A numerical and experimental study of mass transfer in spacer-filled channels: Effects of spacer geometrical characteristics and schmidt number, Journal of Membrane Science 326 (1) (2009) 234 – 251. doi:http://dx.doi.org/10.1016/j.memsci.2008.10.007.

[26] J. Howell, Membranes in Bioprocessing: Theory and Applications, Springer-Sicence+Buisiness Media, B.V, 1993.

[27] C. Williamson, Vortex dynamics in the cylinder wake, Annual Review of Fluid Mechanics 28 (1996) 477–539.

[28] M. Sahin, R. G. Owens, A numerical investigation of wall effects up to high blockage ratios on two-dimensional flow past a confined circular cylinder, Physics of Fluids 16 (2004) 1305. doi:http://dx.doi.org/10.1063/1.1668285.

[29] G. Schock, A. Miquel, Mass transfer and pressure loss in spiral wound modules, Desalination 64 (1987) 339 – 352. doi:http://dx.doi.org/10.1016/0011-9164(87)90107-X.

[30] J. Schwinge, D. E. Wiley, D. F. Fletcher, Simulation of the flow around spacer filaments between narrow channel walls. 1. hydrodynamics, Industrial & Engineering Chemistry Research 41 (12) (2002) 2977–2987. arXiv:http://dx.doi.org/10.1021/ie010588y, doi:10.1021/ie010588y.

[31] H. Jasak, Error analysis and estimation for the finite volume method with applications to fluid flows, Ph.D. thesis, Imperial College, University of London (1996).

[32] S. V. Patankar, C. H. Liu, E. M. Sparrow, Fully developed flow and heat transfer in ducts having streamwise-periodic variations of cross-sectional area, Journal of Heat Transfer 99 (1977) 180–186.

[33] C.-L. Hwang, L.-T. Fan, Finite difference analysis of forced-convection heat transfer in entrance region of a flat rectangular duct, Applied Scientific Research, Section A 13 (1) (1964) 401–422. doi:10.1007/BF00382066.

[34] A. Lévêque, Les Lois de la transmission de chaleur par convection, Dunod, 1928.

[35] A. Haji-Sheikh, J. Beck, D. E. Amos, Axial heat conduction effects in the entrance region of parallel plate ducts, International Journal of Heat and Mass Transfer 51 (2526) (2008) 5811 – 5822. doi:http://dx.doi.org/10.1016/j.ijheatmasstransfer.2008.04.056.

[36] B. M. Sumer, J. Fredsoe, Hydrodynamics around cylindrical structures, 2006.

[37] M. Mahdavi, M. Sharifpur, J. Meyer, {CFD} modelling of heat transfer and pressure drops for nanofluids through vertical tubes in laminar flow by lagrangian and eulerian approaches, International Journal of Heat and Mass Transfer 88 (2015) 803 – 813. doi:http://dx.doi.org/10.1016/j.ijheatmasstransfer.2015.04.112.

[38] M. Turkyilmazoglu, Anomalous heat transfer enhancement by slip due to nanofluids in circular concentric pipes, International Journal of Heat and Mass Transfer 85 (2015) 609 – 614. doi:http://dx.doi.org/10.1016/j.ijheatmasstransfer.2015.02.015.

[39] J. Schwinge, D. E. Wiley, D. F. Fletcher, Simulation of the flow around spacer filaments between channel walls. 2. mass-transfer enhancement, Industrial & Engineering Chemistry Research 41 (19) (2002) 4879–4888. doi:10.1021/ie011015o.

[40] J.-H. Chen, W. Pritchard, S. Tavener, Bifurcation for flow past a cylinder between parallel planes, Journal of Fluid Mechanics 284 (1995) 23–41.

[41] C. Koutsou, S. Yiantsios, A. Karabelas, Numerical simulation of the flow in a plane-channel containing a periodic array of cylindrical turbulence promoters, Journal of Membrane Science 231 (12) (2004) 81 – 90. doi:http://dx.doi.org/10.1016/j.memsci.2003.11.005.